CrystEngComm

Cite this: *CrystEngComm*, 2012, **14**, 397

www.rsc.org/crystengcomm

COMMUNICATION

Facile synthesis of germanium–graphene nanocomposites and their application as anode materials for lithium ion batteries†

Jinsheng Cheng*[ab] and Jin Du[a]

Received 22nd September 2011, Accepted 4th November 2011
DOI: 10.1039/c1ce06251d

A simple and low-cost method to synthesize Ge nanoparticles/graphene (Ge NPs/GR) nanocomposites under mild conditions was developed. The reduction of sugarcane bagasse (SB) derived graphene oxide nanosheets was accompanied by generation of Ge NPs in one step. The resulting nanocomposites exhibit high specific capacity and superior capacity retention of 90% after 15 cycles.

There has been increasing research interest in the development of environmentally benign, long-life, low-cost, renewable and high-capacity batteries,[1–3] especially reliable lithium-ion batteries (LIBs) with high energy and power density in popular consumer devices, such as mobile phones, laptops and hybrid electric vehicles, *etc.*[4,5] In order to further improve the LIBs performance, the development of higher-capacity anodes is required since the commercial graphite anode only has a theoretical capacity of 372 mA h g^{-1}.[6] Recently, group IV semiconductor materials, especially silicon (Si) and germanium (Ge), have attracted great interest in the field of LIBs because of their huge theoretical capacities (Si 4200 mA h g^{-1} and Ge 1600 mA h g^{-1}).[7–9]

Compared with Si, Ge exhibits a 400 times higher room-temperature diffusivity of Li and a lower specific volume change during the Li ion insertion/extraction process.[6,10,11] Therefore, Ge can be expected to exhibit a better cycling performance at comparable capacity as anode material for high-power-rate LIBs. Nevertheless, despite the huge capacity, the fully lithiated $Li_{4.4}Ge$ still undergoes a volume change of 370%, leading to pulverization and capacity fading in bulk electrodes.[12,13] Recently, many strategies have been implemented to solve this problem, including decreasing the particle size,[14,15] combining with inactive/active matrix,[13,14] synthesizing porous materials,[8,16] coating a shell[17] or carbon encapsulation.[11] These methods were proved effective for their inherent advantages such as high contact surfaces and better accommodation of large strain, *e.g.* Maier *et al.* reported carbon matrix supported Ge NPs, which exhibited highly reversible Li storage behavior.[18] However, most of the methods discussed above were time-consuming and had high energy costs. Some even needed expensive precursors or complicated synthetic procedures. Therefore, a simple, mild and low-cost synthesis route to get nanoscale Ge with enhanced electrochemical performance is urgently needed.

GR holds excellent thermal, mechanical and electronic properties,[19–22] which made GR suppress local stress and large volume expansions/shrinkages during a lithiation/delithiation process and alleviate the aggregation or pulverization problems, and significantly offer an efficient electrically conducting channel and superior matrix for growing NPs. Therefore, by combining with GR, the Ge NPs/GR nanocomposites could have enhanced electron transport rate, structural stability, high surface area, chemical inertness and flexibility, which would be promising materials for various kinds of market demanded LIBs.

To date, only very limited reports have been demonstrated on the preparation of Ge NPs/GR composites.[23] Moreover, few reports were presented on the electrochemical performance of Ge NPs/GR. Herein, we demonstrate a simple and mild method to fabricate Ge NPs/GR composites. The GR matrix with superior electronic properties is not only helpful in stabilizing Ge NPs, but also significantly amortizes the volume expansion during charge/discharge and enhances their electronic conductivity, leading to enhanced electrochemical performance as anode materials.

The graphene precursors: graphene oxide (GO)[22,24] was prepared from waste SB derived graphite[25,26] (see ESI†). The reduction of GO nanosheets was accompanied by generation of Ge NPs in one-step. The route to synthesize the Ge NPs/GR composites is shown in Scheme 1. Firstly, the oxygen-containing groups on GO can also provide plentiful sites to anchor Ge(IV) ions and make them enrich in some places. Consequently, the Ge(IV) ions (positive) can be absorbed on GO (negative) readily by electrical interaction.[24] Secondly, the GO nanosheets and Ge ions can be reduced *in situ* by the sodium powder, resulting in Ge NPs loading on graphene nanosheets. GR was also prepared for comparison.

The *Bragg* reflections at 32.5°, 46°, 57° and 67.5° of XRD measurement can correspond to the indexed planes of the crystals of Ge (201), (301), (320) and (430), respectively (JCPDS no. 72-1089, Fig. 1C). The thermal behaviors of the Ge NPs/GR composites were investigated by thermogravimetric analysis (TGA) in dry air (Fig. 1D), which exhibit two steps of mass loss at 200 and 650 °C, respectively.

The morphology and microstructures of GR and Ge NPs/GR were analyzed by TEM. As shown in Fig. 1A, the wrinkled structures

[a]*School of Pharmacy, Guilin Medical University, Guilin, 541004, China*
[b]*Department of Chemistry, Key Lab of Bioorganic Phosphorus Chemistry & Chemical Biology, Tsinghua University, Beijing, 100084, China. E-mail: chengjs@mail.ustc.edu.cn; Tel: +86 773 2295100*

† Electronic supplementary information (ESI) available: Detailed experimental section, supplementary TEM images, EDS analysis, CV curves and voltage–capacity profiles. See DOI: 10.1039/c1ce06251d

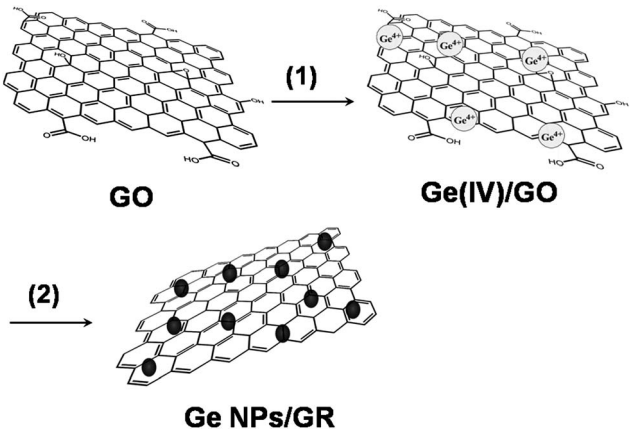

Scheme 1 Schematic illustration of the preparation of Ge NPs/GR nanocomposites. (1) Dispersion and adsorption of Ge ions on graphene oxide nanosheets and (2) one-step reduction of graphene oxide and Ge ions leading to the formation of Ge NPs/GR nanocomposites.

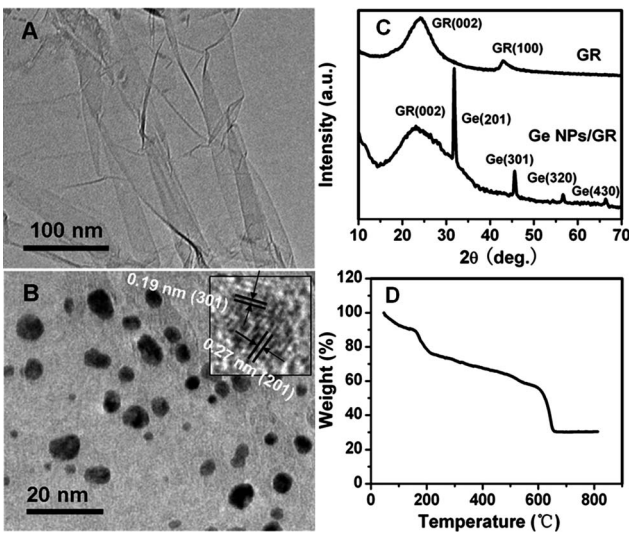

Fig. 1 Characterization of GR and Ge NPs/GR. TEM images of GR (A) and Ge NPs/GR (B), the inset is the lattice structure of Ge NPs. XRD spectra (C) of GR and Ge NPs/GR, and TGA curve (D) of Ge NPs/GR.

of GR could not only enlarge its surface area to help absorb and enrich the Ge ion, but hold the reduced Ge NPs and prevent their aggregation. The typical TEM images of Ge NPs/GR (Fig. 1B and S1A†) show that the Ge NPs with diameters in the range of 2–10 nm are deposited on the basal planes of graphene with wrinkles, and especially, smaller than the exciton Bohr radius of Ge (24.3 nm). Therefore, the Ge NPs in this work can be considered as Ge quantum dots (QDs).[27] The resulting quantum confinement effects can induce electron wave function localization in anode NPs and cause weaker interaction between Li defect and its host, therefore, reduce the diffusion barrier of Li ions with the NPs size decreased, leading to the enhanced electrochemical performance as the anode material.[28] The inset image in Fig. 1B indicates clear evidence of polycrystalline structures of Ge, in which the arrows show the lattice spacing of 0.27 nm and 0.19 nm, similar to the Ge (201) and Ge (301) lattice spacing. The energy dispersive X-ray spectroscopy (EDS) in Fig. S1B† shows the Ge features supported on GR.

Here, cyclic voltammograms (CVs), galvanostatic discharge/charge and impedance experiments were carried out to evaluate the electrochemical performance of Ge NPs/GR used as the anode material in the LIBs. All the electrochemical tests *versus* Li were done in Swagelok-type cells.

The initial three cycles of CV tests of GR, Ge and Ge NPs/GR electrodes were conducted at a fixed potential ranging from 0 V to 2 V with a scan rate of 0.1 mV s^{-1}. Fig. S2A† (see ESI†) shows that by combining the Ge NPs, the lithium capacity of Ge NPs/GR was much larger than that of GR, and more stable than that of the mere Ge NPs. In the first cycle, there is no obvious reduction peak, which may be due to the irreversible reaction and the formation of a solid electrolyte interface (SEI) layer. From the second cycle of Ge NPs/GR electrode, one could observe two broad reduction peaks at about 0.60 and 1.4 V respectively. The former peak corresponds to the formation of Li_xGe and the latter peak is associated with lithium reactions with the carbon.[18] During all the 15 cycles, the two broad peaks kept quite consistent (see ESI, Fig. S2A and D†), indicating the superior structure stability of the Ge NPs/GR nanocomposites. As a comparison, though Ge had large capacity, it could not keep consistent for the first three cycles (Fig. S2B†). Similarly, as indicated in Fig. S2A†, Ge NPs/GR nanocomposites kept the characteristic broad peak at 0.25 V (relevant to Ge NPs) during the cycles, while that of Ge NPs became much weaker (Fig. S2B†), which indicates that the structure of Ge NPs collapsed. Such results further confirm the structure stability of the Ge NPs/GR nanocomposites as the anode materials.

From the discharge curves, the discharge plateau was located near 0.2 V which was matched well with previous works.[29] The specific capacities of GR, Ge and Ge NPs/GR composites are shown in Fig. 2A. In the first cycle, the discharge capacity was extraordinarily large due to formation of the SEI layer. The second charge capacity of the Ge NPs/GR was 738 mA h g^{-1} at the current density of 200 mA g^{-1}, implying an extraordinarily high capacity that may be due to their nanosized nature. After 15 cycles, GR had capacity about 54% (170 mA h g^{-1}) and Ge had about 24% (116 mA h g^{-1}) retention of the second capacity, both fading faster than that of graphite shown in ref. 29, whereas Ge NPs/GR composites showed about 72% retention (532 mA h g^{-1}) for the second capacity. Considering the capacity fading caused by graphene content, the Ge NPs achieved a capacity retention of 88%, which is an excellent result for this kind of lithium alloy anode materials (Si, Ge, Sn, *etc.*).[6]

Coulombic efficiencies at the initial cycles (Fig. 2A, hollow plot), respectively, indicate that the capacity loss for Ge NPs (25%) and graphene (24%) was significantly larger than that for Ge NPs/GR (41%) due to the SEI films, and surface structures of Ge NPs/GR were more stable than those of Ge NPs and GR.[29] The coulombic efficiency of Ge NPs for the second cycle was only 59% and became stable at the seventh cycle. This may be related to the fact that without graphene support, serious agglomeration of the Ge NPs would occur during Li-ions insertion/extraction, leading to irreversibility of the electrode and capacity fading of Ge NPs in the cycles. The GR sample exhibits 80% coulombic efficiency for the second cycle and attains stability at the sixth run, which shows also better performance than that of commercial Ge NPs, indicating the advantages of GR as the electrode materials' support. Moreover, in the Ge NPs/GR sample, the coulombic efficiency of Ge NPs/GR increased to 90% at the second cycle and attained stable status in the subsequent cycles. In this situation, GR nanosheets could limit the

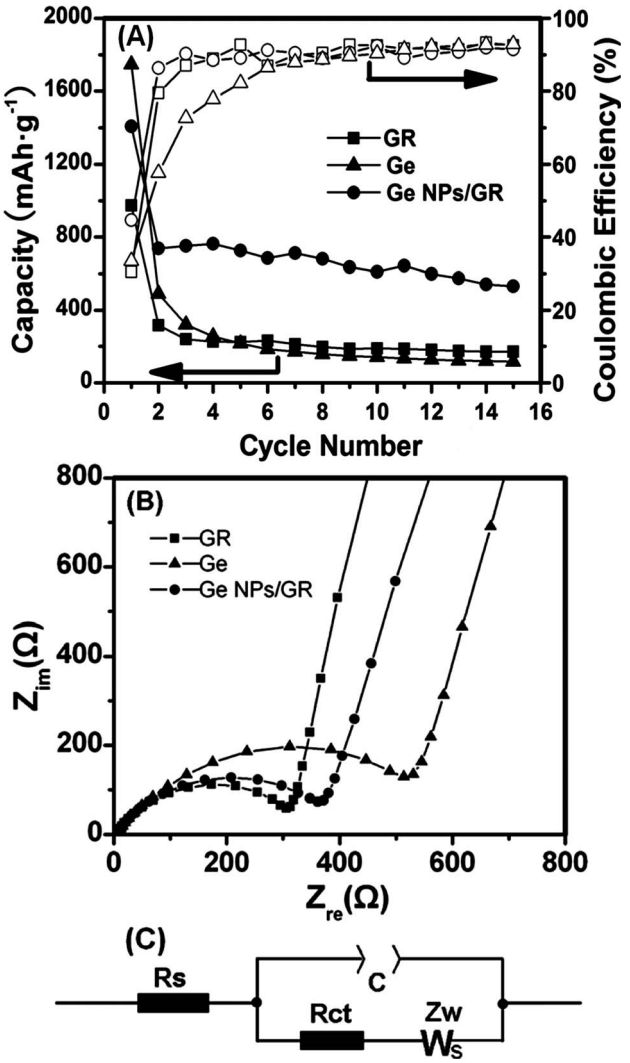

Fig. 2 (A) The specific capacity (solid plot) and coulombic efficiency (hollow plot) performances of GR (■), Ge (▲) and Ge NPs/GR (●). Voltage window: 1 mV to 3 V (*vs.* Li/Li^+); current rate: 200 mA g^{-1}. (B) Nyquist plots of GR (■), Ge (▲) and Ge NPs/GR (●) at the open circuit potential. Frequency range: 100 mHz to 100 kHz. (C) Equivalent circuit mode plot; R_s, resistance of the electrolytes; R_{ct}, charge-transfer resistance; Z_w, Warburg resistance; C, constant phase element.

volume expansion of Ge NPs upon lithium insertion. Therefore the stress produced during the process of lithium insertion was avoided effectively. Even when the volume expansion had happened, the electrode was hard to pulverize and exfoliate because the planar graphene surface had enough void spaces and wrinkles to hold the expanded or broken NPs. This would greatly improve the electrode materials' stability and adaptability in the cycles. Above points were confirmed by TEM images of fully charged and discharged Ge NPs/GR electrodes (see ESI, Fig. S1C and D†).

The electrochemical impedance spectra of GR and Ge NPs/GR are demonstrated in Fig. 2B. As shown in the curves, the impedance spectra consist of a semicircle in the high frequency region and an inclined straight line in the low frequency region. The semicircle in the middle frequency region is attributed to the charge-transfer resistance (R_{ct}), relating to the charge transfer through the electrode/electrolyte interface. The inclined line corresponds to solid-state diffusion of lithium-ion (Warburg impedance) in the electrode materials. The intercept at Z_{re} in high frequency regions is related to the resistance of the electrolytes (R_s). The impedance spectra can be analyzed with the same simple equivalent circuit mode (Fig. 2C). A constant phase element (C) was used instead of the double layer capacitance. From the Nyquist plots, it can be found that the radius of the semicircle of the Ge NPs/GR electrode was close to GR and much smaller than that of the Ge electrode. The results indicate that R_{ct}, C and Z_{re} of the Ge NPs/GR electrode were smaller than those of the Ge electrode and close to the GR electrode, which could prove that GR would provide an improvement to the conductivity of the electrode.

In conclusion, we have developed a simple, convenient and low-cost method to fabricate Ge NPs/GR nanocomposites under mild conditions. The reduction of SB derived graphene oxide nanosheets was accompanied by generation of Ge NPs in one-step. The graphene nanosheets are not only helpful in stabilizing Ge NPs, but also significantly enhancing their electronic conductivity and electrochemical performance as the high-capacity anode material for LIBs. The resulting nanocomposites exhibit high specific capacity and superior capacity retention of 90% after 15 cycles, indicating their potential application as promising candidates for the development of low-cost and high-performance LIBs.

This work was financially supported by the Guangxi Zhuang Autonomous Region Science Foundation of China (no. 200908193).

Notes and references

1 B. Scrosati, *Nature*, 1995, **573**, 557–558.
2 M. S. Whittingham, *Chem. Rev.*, 2004, **104**, 4271–4301.
3 Z. H. Wen, Q. Wang, Q. Zhang and J. H. Li, *Adv. Funct. Mater.*, 2007, **17**, 2772–2778.
4 C. M. Park, J. H. Kim, H. Kim and H. J. Sohn, *Chem. Soc. Rev.*, 2010, **39**, 3115–3141.
5 H. Li, Z. X. Wang, L. Q. Chen and X. J. Huang, *Adv. Mater.*, 2009, **21**, 4593–4607.
6 J. Graetz, C. C. Ahn, R. Yazami and B. Fultz, *J. Electrochem. Soc.*, 2004, **151**, A698–A702.
7 C. Chan, H. L. Peng, G. Liu, K. McIlwrath, X. F. Zhang, R. A. Huggins and Y. Cui, *Nat. Nanotechnol.*, 2008, **3**, 31–35.
8 M. Park, K. Kim, J. Kim and J. Cho, *Adv. Mater.*, 2010, **22**, 415–418.
9 S. H. Ng, J. Z. Wang, D. Wexler, K. Konstantinov, Z. P. Guo and H. K. Liu, *Angew. Chem., Int. Ed.*, 2006, **45**, 6896–6899.
10 C. K. Chan, X. F. Zhang and Y. Cui, *Nano Lett.*, 2008, **8**, 307–309.
11 S. Yoon, C. Park and H. Sohn, *Electrochem. Solid-State Lett.*, 2008, **11**, A42–A45.
12 P. Teki, M. K. Datta, R. Krishnan, T. C. Parker, T. M. Lu, P. N. Kumta and N. Koralkar, *Small*, 2009, **5**, 2236–2242.
13 U. Kasavajjula, C. S. Wang and A. J. Appleby, *J. Power Sources*, 2007, **163**, 1003–1039.
14 M. G. Kim and J. Cho, *J. Electrochem. Soc.*, 2007, **156**, A277–A282.
15 H. Lee, H. Kim, S. G. Doo and J. Cho, *J. Electrochem. Soc.*, 2007, **154**, A343–A346.
16 L. C. Yang, Q. S. Gao, L. Li, Y. Tang and Y. P. Wu, *Electrochem. Commun.*, 2010, **12**, 418–421.
17 H. Lee and J. Cho, *Nano Lett.*, 2007, **7**, 2638–2641.
18 G. L. Cui, L. Gu, L. J. Zhi, N. Kaskhedikar, P. A. V. Aken, K. Müllen and J. Maier, *Adv. Mater.*, 2008, **20**, 3079–3083.
19 A. K. Geim, *Science*, 2009, **324**, 1530–1534.
20 J. K. Lee, K. B. Smith, C. M. Hayner and H. H. Kung, *Chem. Commun.*, 2010, **46**, 2025–2027.
21 C. J. Xu, J.-H. Lee, J.-C. Lee, B.-S. Kim, S. W. Hwang and D. Whang, *CrystEngComm*, 2011, **13**, 6036–6039.
22 J. S. Cheng, L. H. Tang and J. Y. Xu, *J. Mater. Chem.*, 2011, **21**, 3485–3494.
23 S. D. Park, S. W. Lee, S. Kang, I. C. Bang, J. H. Kim, H. S. Shin, D. W. Lee and D. W. Lee, *Appl. Phys. Lett.*, 2010, **97**, 3–6.

24 W. S. Hummers and R. E. Offeman, *J. Am. Chem. Soc.*, 1958, **80**, 1339–11339.
25 M. Ruiz and C. Rolz, *Ind. Eng. Chem. Prod. Res. Dev.*, 1971, **10**(4), 429–432.
26 B. S. Girgis, L. B. Khalil and T. A. M. Tawfik, *J. Chem. Technol. Biotechnol.*, 1994, **61**, 87–92.
27 G. Gu, M. Burghard, G. T. Kim, G. S. Düsberg, P. W. Chiu, V. Krstic and S. Roth, *J. Appl. Phys.*, 2001, **90**, 5747–5751.
28 T. L. Chan and J. R. Chelikowsky, *Nano Lett.*, 2010, **10**, 821–825.
29 Z. G. Lu, H. Cheng, M. F. Lo and C. Y. Chung, *Adv. Funct. Mater.*, 2007, **17**, 3885–3896.

